2021 43rd Annual International Conference of the
IEEE Engineering in Medicine & Biology Society (EMBC)
Oct 31 - Nov 4, 2021. Virtual Conference

Computer Aided Image Processing to Facilitate Determination of Congruence in Manual Classification of Mitochondrial Morphologies in *Toxoplasma gondii* Tissue Cysts*

Brooke C Place[1], Cortni Troublefield[2], Robert D. Murphy[2], Anthony P. Sinai[2], and Abhijit Patwardhan[1#], [#]Member, *IEEE*

***Abstract*— *Toxoplasma gondii* is a parasite that chronically infects about a third of the world's population. During chronic infection, the parasite resides within tissue cysts in the form of poorly understood bradyzoites which can number in the thousands. Our prior work showed that these bradyzoites are metabolically active exhibiting heterogeneous replication potential. The morphological plasticity of the mitochondrion potentially informs about parasite metabolic state. We developed an image processing based program to assist manual classification of mitochondrial morphologies by trained operators to collect data and statistics from the manual classification of shapes. We sought to determine whether certain morphologies were readily classifiable and the congruence among manual classifiers, i.e. the degree to which different operators would place the same objects within the same class. Results from three operators classifying mitochondrial morphologies from 5 tissue cyst images showed that among the four classes, one (Blobs) were the easiest to classify. There was remarkable congruence between 2 of the 3 operators in classifying the objects (96%), while the agreement among all 3 operators was somewhat modest (57%). Such information would be valuable for biologists studying these parasites as well as in development of fully automated methods of morphological classification.**

I. Introduction

Toxoplasma gondii, a protozoan parasite, chronically infects about a third of the world's population causing symptomatic disease in the immune compromised [1]. During the acute infection, the parasite is in a rapidly dividing form called a tachyzoite which is controlled by a healthy immune system [1]. However, instead of being completely cleared, some parasites evade the immune system by transitioning to the poorly understood bradyzoite form within tissue cysts establishing a life-long infection [1, 2]. These cysts are typically located in the central nervous system and muscles [2]. Reactivation of these forms in the context of immune suppression causes life-threating conditions including toxoplasmic encephalitis and disseminated toxoplasmosis [1, 3].

The approaches for studying *T. gondii* during the chronic infection have been based on the assumption that the bradyzoites within the cysts are largely dormant, with all analysis viewing the tissue cyst as the unit of infection. Prior work from our group showed that the bradyzoites within the cysts are not dormant but rather capable of replication that is heterogeneous within cysts [4]. This observation suggests the need for investigating the biology of the parasite during chronic infection at the level of individual bradyzoites, which can number in the hundreds to several thousand [4], rather than that of the cysts that house them. To achieve this 2-3 log increase in sensitivity there is a need for more robust tools to evaluate physiological heterogeneity. While programs have been developed to aid the analysis of host response via protein recruitment [5] and the analysis of the tissue cyst morphology [6], detailed analysis has not been performed at the level of the individual bradyzoites and further, at the level of organelles within them. To build upon the previous finding that the bradyzoites are not dormant and are actually metabolically active with heterogeneous replication, investigation of functional state of mitochondria, among other processes, is necessary, as mitochondrial function directly informs about the metabolic activity of bradyzoites [7]. *T. gondii* tachyzoites, associated with the acute infection, possess a single large mitochondrion [8]. Previous work, in tachyzoites, has shown that morphology of this mitochondrion is plastic, reflecting its physiological state [9, 10]. These morphologies include a lasso (ring), arcs (linear and curvilinear forms), tadpoles (also termed sperm-like) and blobs (also termed collapsed) forms [9, 10]. In addition, under conditions of nutrient stress and drug pressure, the mitochondrion can be fragmented into multiple puncta [9, 11].

In contrast, little is known about the morphology of mitochondria within encysted bradyzoites. Given the heterogeneity of the bradyzoites, manual classification of mitochondrial profiles presents challenges as this process is time consuming, subject to tedium and thus error. We developed an image processing based program to assist manual classification of morphologies by trained operators as an initial step toward the eventual development of image processing and machine learning approaches to automatically classify mitochondrial morphologies. The purpose of the development described here was to collect data and statistics from manual classifications of mitochondrial shapes to determine whether certain morphologies were readily classifiable and the congruence among manual classifiers, i.e. the degree to which different operators would place the same objects within the same class.

II. Materials and Methods

A. Image Input

First, tissue cysts of the Type II ME49 strain were purified

*Research supported by National Institute of Health grant R01AI145335 awarded to APS and AP (MPI's).
Authors are with the [1]College of Engineering, [2]College of Medicine, University of Kentucky, Lexington, KY 40506 USA
address correspondence to e-mail: abhijit.patwardhan@uky.edu

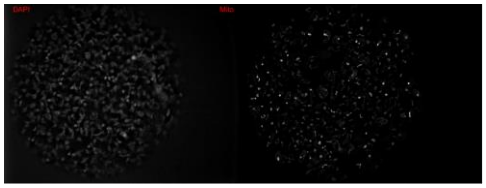
Figure 1. A representative DAPI (left) and Mito (right) image.

from brains of chronically infected CBA/J mice using a Percoll gradient as previously described [12]. All experimental procedures involving use of animals were approved by the Institutional Animal Care and Use Committee at the University of Kentucky. The purified tissue cysts were labeled with a DNA dye (DAPI, Invitrogen) and MitoTracker red (Invitrogen) to target two subcellular entities, nuclei (DAPI) and actively respiring mitochondria (Mito). The cysts were fixed in 3% paraformaldehyde and deposited on glass slides, cover-slipped and imaged. The z-plane image with the widest diameter for each cyst was designated as the representative image to be used in the analysis. The images were acquired on a Zeiss Axioplan microscope using a 100x/1.4 numerical aperture objective using a grayscale AxioCam MRM digital camera. The resulting magnification in images was 15.5 pixels per micron. Examples of DAPI and Mito images are shown in Fig. 1.

B. Image Processing and Segmentation

A program was developed in MATLAB using its Image Processing toolbox and its App Designer was used in the creation of a graphical user interface (GUI) [13]. The GUI allowed for the creation of a user-friendly method to facilitate the classification of mitochondrial morphologies within cysts.

First, a linear intensity scaling was performed on the 8 bit grayscale image such that the pixel intensities occupied the full range (0-255). Enhancing the contrast between the background pixels and the target objects' pixels was then performed utilizing top hat and bottom hat filters [14]. The two filters were used in conjunction as described in (1). The foreground was emphasized by the addition of the top hat filter to the original image, I, which made the bright spots brighter. The objects' perimeter was enhanced by the subtraction of the bottom hat filtered image.

$$[J]=\text{Tophat}[I]+[I]-10*\text{Bottomhat}[I] \quad (1)$$

Next, thresholding was used to separate foreground and background pixels. The Otsu method was used to obtain an initial estimate of the threshold [15]. A slider feature was added to the program so that the operator could modify the initial selection of threshold, if needed, to ensure the target objects were segmented as accurately as possible.

After the evaluation of a few images the initial estimates of threshold were selected as 40% of the Otsu threshold for Mito images and 80% of the Otsu threshold for the DAPI images. The DAPI images required a higher percentage of the Otsu threshold which resulted in the exclusion of a greater number of lower value pixels. This exclusion prevented under segmentation in the DAPI images where the individual target objects were less defined. Following thresholding, watershed segmentation [16] was applied to the DAPI images to segment the target objects more accurately, especially those within proximity of each other. To prevent over segmentation which can happen with the watershed method, it was implemented after using a height transform to suppress smaller peaks, therefore peaks of one standard deviation of image pixel values or less were ignored.

C. Object Identification

Using the selected threshold, the Mito images were binarized, i.e. the pixels with intensity values above the threshold were given a value of 1 while the remaining pixels were set to 0, creating a binary image. The Moore-Neighbor tracing algorithm with Jacob's stopping criterion [14] was then used to locate the boundary of each object of interest. Geometric and pixel value information for the identified objects were extracted with the use of various functions such as 'regionprops' in Matlab [13]. Two criteria were applied to the identified objects to exclude objects that were smaller than a certain size and dimmer than a certain threshold (but with intensity above the binarization threshold). Minimum axis length and maximum intensity within each object were used to compare against user selected size and intensity thresholds. This step allowed for the exclusion of objects that had a minor axis, or width, less than a specific value in microns. This 'low size' exclusion criterion was defaulted to half a micron, i.e. seven pixels. Dimmer objects that may result from over segmentation could be excluded with the intensity criterion. The default threshold for this 'low intensity' exclusion criterion was set to be the same value as the threshold found for creating the binary image, therefore it did not initially exclude any objects. These exclusion criteria were displayed in the GUI for the operator to update as needed.

Previous work has highlighted four main classes of mitochondrial morphology in tachyzoites that have association with function, these are punctate/condensed (blob), tadpole/sperm-like, arc (linear, curvilinear, loop), and lasso (ring) shapes [9, 10]. The main purpose of this development, in addition to capturing manual classification, was to determine whether the morphologies were a) readily identifiable, i.e. whether operators with varying degrees of experience would classify the object the same way, and b) the congruence, i.e. degree of agreement, among different operators in classifying the same objects. Therefore, buttons were added to the GUI alongside the isolated target objects' image to collect this information. An additional 'Other' class was added for objects that the operator could not place in any one of the four specified classes. This was particularly important as nothing has been described about the morphological diversity of mitochondrial profiles in encysted bradyzoites.

D. Capture of Operator Classification Data

To evaluate the manual classification process, the program was set up to allow for the input of a settings file containing the image file information along with the threshold and exclusion criteria selections that a single lead operator had previously specified. This step ensured that the different operators were presented with the same objects for classification.

Fig. 2 shows the layout of the GUI. The workflow in identifying and classifying the mitochondrial morphologies is as follows: Bradyzoites contain a single nucleus and, based on what is known about tachyzoites, they are expected to contain

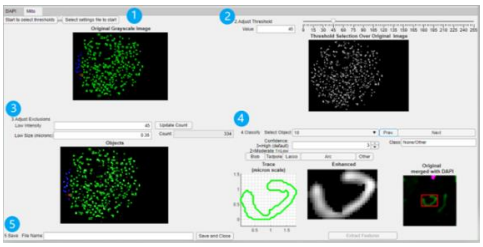

Figure 2. Mito tab of the GUI with numbers representing the sequential steps to be taken: 1) selecting the button to begin settings selection or the button to load a settings file, 2) adjusting the threshold setting, 3) adjusting the exclusion criteria, 4) classifying the object morphology, and 5) saving the output files.

a single mitochondrion [8]. The number of nuclei identified from the DAPI stained images serves as a reference for the number of mitochondrial objects detected in Mito images, therefore, the operator first selects the DAPI tab which displays the DAPI image. Original DAPI image and a binarized version using the default threshold (based on Otsu algorithm) and the number of identified nuclei (after application of height transform and watershed segmentation) are displayed, the operator then adjusts the threshold along with the exclusion criteria, if needed. The Mito tab is selected next which results in a display as shown in Fig. 2. The initial view includes the objects (marked by a green bounding box that surrounds each object) identified using the default threshold. The operator then adjusts the threshold by utilizing the ability to zoom in on the images shown in the top row. After this step, the low size and intensity exclusion criterion are adjusted if needed. After every adjustment, the 'Update Count' button is clicked after which the updated number of objects is displayed in the 'Count' box. If the number of identified and retained objects exceeds the number of identified nuclei in the DAPI image, the number in the 'Count' box is displayed in red color, which serves as a reference in selection of parameters because as stated before, in this parasite the number of mitochondrial objects is generally expected to be similar to the number of nuclei. As MitoTracker records only active mitochondria, the presence of "inactive" mitochondria can result in the number of objects recorded being lower than that for DAPI-stained nuclei. Likewise extensive mitochondrial fragmentation [9] could result in a higher relative mitochondrial count, although such fragments would be typically excluded using the size criteria. Each identified object after the application of exclusion criteria, simply referred to as "objects" from here on, is displayed within a bounding box as shown in the two panels on the left in Fig. 2.

For the classification process, objects are displayed in the 3 panels in the lower right as shown in Fig. 2. The first panel shows the outline or boundary of the object with grid lines (scaled in microns) for ease of visualization and assessment of the object's size. The second panel shows the contrast enhanced object. The third panel shows a 6x6 micron area (centered on the center of the object) from the processed DAPI image (in magenta) superimposed on the same area from the original Mito image. This third panel provides the operator a combined view of the objects' neighborhood from both images such that proximity and placement/orientation of the object relative to neighboring nuclei can be considered in classifying the object. After visualizing the provided information, the operator then selects the object's class as either Blob, Tadpole, Lasso or Arc by clicking on the appropriate button. If the operator cannot place the object in any of these 4 classes, then the 'Other' button is clicked. The operator also has an option of selecting the confidence that they have in classifying that object among High, Medium, or Low. The confidence is set to default to High. Once the appropriate class button is clicked, the program automatically displays the next object, although any of the previously classified objects can be revisited by using the previous and next buttons or directly selecting an object number using a dropdown menu.

To keep track of overall progress, the bounding boxes surrounding each object change color from green to red for the object under consideration for classification and turn blue once the object is classified. The change in color also assists the operator for taking a zoomed in look, if necessary, at the object in the original image shown in the top left panel.

Feedback from the eventual operators was sought throughout the iterative development process and was incorporated in the GUI design to ensure ease of use. For instance, for the selection of threshold step, it was suggested that it would help to have a separate larger window of the thresholded image to evaluate the effects of adjusting the threshold. Therefore, the image under the threshold slider was also displayed in a separate window that would update every time the threshold was updated. This image depicted not only the pixels that exceeded the threshold, but also displayed the original image with an outline of what was retained when the threshold was applied. Further, for ease of identification of the object with respect to the original image, the bounding boxes in the binary image were replicated on the original image (top left panel).

III. Results

Three operators manually classified objects from 5 images. There was a total of 1,138 objects that were identified (after application of exclusion criterion) and classified. Of the 1,138 objects, 649 were placed in the same class by all 3 operators, i.e. 57% of the objects were classified similarly by all operators. A total of 1,092 objects (96%) were classified as belonging to the same class by 2 out of the 3 three operators.

Fig. 3 shows the classification for the first 50 objects (of 1,138) made by the 3 operators. The figure shows that Blobs were more likely to be classified similarly by all 3 operators followed by Arc, Tadpole and Other. There were very few Lassos classified and there was heterogeneity of opinion about Lasso classification. Notably, Lassos are associated with actively replicating parasites [9, 10] that are infrequent in bradyzoites [4].

Results from the entire data set, in Fig. 4, show that Blobs were the most frequent class to occur and were also most likely to be uniformly recognized by all operators. Arcs were the next

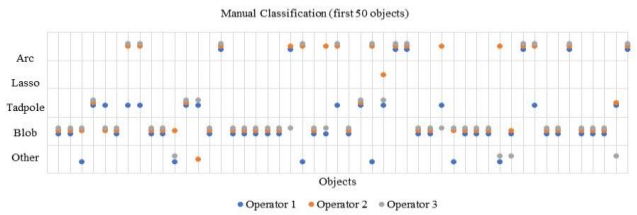

Figure 3. Manual classifications made by each operator for first 50 objects.

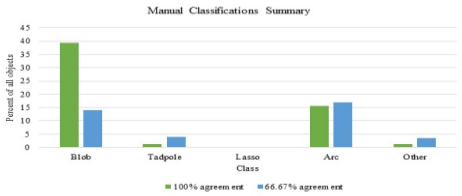

Figure 4. Percentage of all objects classified separated by class chosen and the percent agreement between operators.

class, followed by Tadpole and then Lasso. The number of objects that could not be classified was comparable to that of Tadpoles. About equal numbers of classified Arcs were done so by all three as was done by two operators. Very few Tadpoles were classified as such by all three operators and there was no uniformity of opinion for selection of Lasso.

TABLE I. OPERATOR AGREEMENT COMPARISON

Operator	*1 VS 2*	*1 VS 3*	*2 VS 3*
Count	810	735	856
Percent (%)	71	65	75

Visual inspection of classified objects showed that even within the same class, there was considerable diversity of morphologies. A comparison of how one operator agreed with another is shown in Table 1. The table shows that operator 1 agreed with operator 2 and operator 3 for 71% and 65% of the objects that were classified, while operator 2 and operator 3 agreed for 75% of the objects that were classified. Generalized Kappa as defined by Fleiss [17], computed for the classifications by the three operators was 0.51. Using the qualitative scale suggested by Landis [18], this value of Kappa indicates a moderate degree of agreement amongst operators.

IV. DISCUSSION

Previous findings suggest that bradyzoites within cysts are not completely dormant, rather are metabolically active with heterogeneous replication [4]. Investigation of mitochondrial function has the potential to inform about the metabolic activity of the bradyzoites, and thus their replication potential within the cysts [2]. Certain mitochondrial morphologies are associated with their functional state [9, 10], hence classification of the morphologies of mitochondria within bradyzoites into one of these shapes would inform about the metabolic state of that bradyzoite. The total number of cysts and number of bradyzoites within these cysts can be in the thousands [4], therefore automated means of classifying mitochondrial morphologies would be very beneficial in the study of the biology of these parasites which would be necessary to develop effective treatments for the chronic infection of this parasite. The purpose of this study was to develop an approach to facilitate manual expert classification of mitochondrial shapes which could be used as a training set in machine learning for the eventual goal of fully automated classification. We also were interested in determining which morphologies were easily classifiable, i.e. their class was readily apparent, and the congruence, i.e. degree of agreement, among different operators in classifying the same objects as this information would be valuable for the biologists as well as during development of automated approaches.

Our results showed remarkable congruence between 2 of the 3 operators in classifying the objects, while the agreement among all 3 operators was somewhat modest. The three operators had varying degree of experience in terms of investigation of mitochondrial function, with one having 25+ years of experience, and the other two with less than 4 and 2 years. Results suggest that, not surprisingly, Blobs are relatively easy to classify as the degree of congruence among operators with varying level of experience was the highest. It is noteworthy that although our prior work shows surprising level of activity in cyst encased bradyzoites, their metabolic activity is still expected to be at a very low level for a large fraction of them. Therefore, the lower incidence of identified Lasso and Tadpole morphologies was not surprising as these are associated with a more active parasite mitochondrion [9].

In summary, results of our study provide information about the degree of congruence among manual classifiers in classifying mitochondrial morphologies which would be valuable in designing machine learning approaches for fully automatic classification by providing not only training sets, but also helping to establish bounds for the expected accuracy of automatic classification compared to manual operators.

REFERENCES

[1] A. M. Tenter, A. R. Heckeroth, and L. M. Weiss, "Toxoplasma gondii: from animals to humans," *Int J Parasitol,* vol. 30, pp. 1217-58, Nov 2000.

[2] A. P. Sinai, E. A. Watts, A. Dhara, R. D. Murphy, M. S. Gentry, and A. Patwardhan, "Reexamining Chronic Toxoplasma gondii Infection: Surprising Activity for a "Dormant" Parasite," *Current Clinical Microbiology Reports,* vol. 3, pp. 175-185, 2016.

[3] A. Nath and A. P. Sinai, "Cerebral Toxoplasmosis," *Curr Treat Options Neurol,* vol. 5, pp. 3-12, Jan 2003.

[4] E. Watts, Y. Zhao, A. Dhara, B. Eller, A. Patwardhan, and A. P. Sinai, "Novel Approaches Reveal that Toxoplasma gondii Bradyzoites within Tissue Cysts Are Dynamic and Replicating Entities In Vivo," *MBio,* vol. 6, pp. e01155-15, 2015.

[5] D. Fisch, A. Yakimovich, B. Clough, J. Wright, M. Bunyan, M. Howell*, et al.*, "Defining host-pathogen interactions employing an artificial intelligence workflow," *Elife,* vol. 8, Feb 12 2019.

[6] N. Bauman, A. Ilic, O. Lijeskic, A. Uzelac, I. Klun, J. Srbljanovic*, et al.*, "Computational image analysis reveals the structural complexity of Toxoplasma gondii tissue cysts," *PLoS One,* vol. 15, p. e0234169, 2020.

[7] W. Bohne, J. Heesemann, and U. Gross, "Reduced replication of Toxoplasma gondii is necessary for induction of bradyzoite-specific antigens: a possible role for nitric oxide in triggering stage conversion," *Infect Immun,* vol. 62, pp. 1761-7, May 1994.

[8] F. Seeber, D. J. Ferguson, and U. Gross, "Toxoplasma gondii: a paraformaldehyde-insensitive diaphorase activity acts as a specific histochemical marker for the single mitochondrion," *Exp Parasitol,* vol. 89, pp. 137-9, May 1998.

[9] D. Ghosh, J. L. Walton, P. D. Roepe, and A. P. Sinai, "Autophagy is a cell death mechanism in Toxoplasma gondii," *Cellular microbiology,* vol. 14, pp. 589-607, Apr 2012.

[10] J. Ovciarikova, L. Lemgruber, K. L. Stilger, W. J. Sullivan, and L. Sheiner, "Mitochondrial behaviour throughout the lytic cycle of Toxoplasma gondii," *Scientific reports,* vol. 7, p. 42746, 2017.

[11] M. D. Lavine and G. Arrizabalaga, "Analysis of monensin sensitivity in Toxoplasma gondii reveals autophagy as a mechanism for drug induced death," *PLoS One,* vol. 7, p. e42107, 2012.

[12] E. A. Watts, A. Dhara, and A. P. Sinai, "Purification Toxoplasma gondii Tissue Cysts Using Percoll Gradients," *Curr Protoc Microbiol,* vol. 45, pp. 20C 2 1-20C 2 19, May 16 2017.

[13] "MATLAB" *R2019a*, MATLAB 9.7 ed: The Mathworks Inc., 2019.

[14] R. C. Gonzalez, R. E. Woods, and S. L. Eddins, *Digital Image processing using MATLAB*. Upper Saddle River, N. J.: Pearson Prentice Hall, 2004.

[15] N. Otsu, "A Threshold Selection Method from Gray-Level Histograms," *IEEE transactions on systems, man, and cybernetics,* vol. 9, pp. 62-66, 1979.
[16] F. Meyer, "Topographic distance and watershed lines," *Signal Processing,* vol. 38, pp. 113-125, 1994/07/01/ 1994.
[17] J. L. Fleiss, "Measuring nominal sclae agreement among many raters," *Psychological Bulletin,* vol. 76, pp. 378-382, 1971.
[18] J. R. Landis and G. G. Koch, "The measurement of observer agreement for categorical data," *Biometrics,* vol. 33, pp. 159-74, Mar 1977.